Brazilian Journal
of Chemical
Engineering

ISSN 0104-6632
Printed in Brazil
www.abeq.org.br/bjche

Vol. 36, No. 04, pp. 1621 - 1630, October - December, 2019
dx.doi.org/10.1590/0104-6632.20190364s20190008

SELECTIVE SEPARATION OF Mn(II) AND Cd(II) AS WELL AS REGENERATION OF POLYMER VIA SHEAR INDUCED DISSOCIATION COUPLING WITH ULTRAFILTRATION

Meng-Yuan Qin[1], Shu-Yun Tang[1] and Yun-Ren Qiu[1*]

[1] Central South University, School of Chemistry and Chemical Engineering, Changsha, China. ORCID: 0000-0002-2032-4884; ORCID: 0000-0003-3841-1668; E-mail: csu_tian@csu.edu.cn - ORCID: 0000-0003-1705-5051

(Submitted: January 9, 2019 ; Revised: March 30, 2019 ; Accepted: April 15, 2019)

Abstract - The selective separation of Mn(II) and Cd(II) as well as regeneration of the complexing agent were conducted by shear induced dissociation coupling with ultrafiltration (SID-UF), and the copolymer of maleic acid and acrylic acid (PMA) was used as complexing agent. At the optimal complexation conditions, pH 6 and P/M (mass ratio of polymer to metal ions) 9, both the rejections of Mn(II) and Cd(II) arrived at more than 99%. The shear stabilities of two PMA-metal complexes at different pHs were particularly investigated using rotating disk membrane and the results indicated that critical shear rates γ_c of PMA-Mn complex were lower than that of PMA-Cd at the same pH. According to the difference of the shear stabilities between PMA-Mn and PMA-Cd complexes, the selective separation of Mn(II) and Cd(II) were achieved by SID-UF at 1450 rpm and 1600 rpm, and PMA was regenerated.
Keywords: Ultrafiltration; Shear stability; Critical shear rate; Selective separation coefficient; Regeneration.

INTRODUCTION

Wastewater containing Mn(II) and Cd(II) originated from manganese mining exploration generally has a low pH (1~3) and involves multiple ingredients such as various organic or inorganic agents, a large amount of suspended substances and other metal ions, which produce a marked impact on the surrounding ecological environment and agricultural production. Excessive intake of this polluted water can cause metal poisoning or even irreversibly harm the human nervous system as well (Sharma, et al., 2007). Before the disposal of manganese mining wastewater, the metal contents should be eliminated (Shafaei, et al., 2010).

The processes available for the treatment of heavy metal wastes such as chemical flocculation, ion exchange, adsorption by porous materials, electrolysis and microbiological degradation are either physico-chemically or biologically based. (Pacini, et al., 2005; Sahabi, et al., 2009; Taffarel and Rubio, 2009; Ye, et al., 2011). Nevertheless, these methods usually produce secondary pollution and are not easy to reuse the metals. Furthermore, they are not suitable for the treatment of effluent with low metal concentration and can not effectively separate different metals. Comparatively, there are several reports about the removal of Cu(II), Cr(III), Ni(II), Mn(II), Pb(II), Cd(II) and other heavy metal ions by polymer-assisted ultrafiltration (PAUF) (Demey, et al., 2017; Molinari, et al., 2004; Molinari, et al., 2006; Zeng, et al., 2012). In PAUF process, the heavy metal ions and polymers can interact to generate complexes with high molecular weight, the unbound metal ions can pass through the membrane, whereas the polymers and complexes are retained (Juang and Shiau, 2000). Owing to the high separation selectivity, high removal efficiency and low energy requirements (Juang and Chiou, 2000; Qiu and Mao, 2013), PAUF has applicability in many areas involving the removal/

* Corresponding author: Yun-Ren Qiu - E-mail: csu_tian@csu.edu.cn

recovery of metal ions from a variety of aqueous streams as well as metal-ion-contaminated solids (Jarvinen, et al., 1999). Nonetheless, after PAUF, the complexing agent and metal resources are generally recovered by acidification-dissociation, which may consume a large amount of water and acid. The inevitable membrane fouling in consecutive PAUF process hinders its industrial application as well. In addition, the rejection rate of target metal ions in PAUF is always lower than 50% in pilot trials, much less than the laboratory result. As previous study reported, macromolecules with longer chains always have a higher risk to be broken due to pump shearing (Geckeler and Volchek, 1996). There is a distinct possibility that the differences of feed pumps cause this result: the high shear rate provided by the blades of the centrifugal pump in pilot trials may break the polymer-metal bonds in complexes, which causes a remarkable decline of the rejection rate (Tang and Qiu, 2018).

In this paper, the shear enhanced PAUF process was applied for the treatment of simulated mining wastewater containing Mn(II) and Cd(II), and a rotating disk membrane (RDM) module was employed and the copolymer of maleic acid and acrylic acid (PMA) with high content of carboxylic groups as well as great water-solubility was used as complexing agent. Shear enhanced filtration is also called dynamic filtration, it consists a rotating disk over the fixed membrane, or a rotating or vibrating membrane (Jaffrin, 2008). In a high shear ultrafiltration system, the rotation of the membrane or the disk induces hydraulic turbulence, which minimizes the deleterious effects of concentration polarization as well as decreases the potential for membrane fouling as the feed solutions are concentrated (Viadero, et al., 2000). Previous studies reported a novel dynamic filtration system equipped with a RDM module (Frappart, et al., 2006; Luo, et al., 2010), and it was found that this system obtained significantly increased permeate flux and effectively improved retention of ions and small solutes. Accordingly, our study tries to simulate the high shear centrifugal pump by rotation of the disk and verify the inner relation between the shear rate and stability of the polymer-metal complex in the shear field. Besides, shear induced dissociation coupled with ultrafiltration (SID-UF) is applied to selectively separate Mn(II) and Cd(II) according to the difference of shear stability between PMA-Mn and PMA-Cd complexes.

In this work, the distribution of shear rate along the membrane radius was investigated. The effects of solution pH, mass ratio of polymer to metal ions (P/M) and rotating speed of disk on the rejections of Mn(II) and Cd(II) were studied. The critical shear rates, at which PMA-Mn and PMA-Cd complexes begin to dissociate, were calculated. The relationship between the critical radius and disk rotating speed was obtained. What is more, the selective separation coefficient of Mn(II) and Cd(II) varied with disk rotating speed at different pHs was explored. The shear induced dissociation coupling with ultrafiltration was finally conducted to selectively separate Mn(II) and Cd(II) as well as regenerate PMA. This work can give a guidance to the application of PAUF and may provide a novel idea for the separation of different heavy metals.

MATERIALS AND METHODS

Experimental set-up

The diagram of experimental device is shown in Fig. 1. In this filtration system, a detachable RDM module is installed inside a 0.088 m inner radius cylindrical housing. A circular disk with six radial vanes is fixed in the end of the driving shaft. The other end of shaft outside the housing is connected with an electromotor that can drive the disk to rotate. A PES (polyethersulfone) flat ultrafiltration membrane (Shanghai Yuling Filtration Equipment Co., Ltd) with an effective area of 0.0253 m^2 (outer radius is 0.088m, inner radius is 0.005 m) and molecular weight cut-off (MWCO) of 30 kDa is fixed on the bottom of the housing cavity. The axial distance between the membrane and disk is 14 mm while the radius and thickness of the circular disk are 83 mm and 4 mm, respectively. The feed is supplied from a 4 L thermostatic bath by a peristaltic pump running at a flow-rate of 150 mL/min (YZ1515, China). A cooling water circulation system is installed in the bearing for cooling the driving shaft and maintaining a constant fluid temperature (25 ± 1 °C) in the housing cavity. Pressure gauges are installed at three points on the back plate of the housing to monitor the pressure, which are 0.029 m, 0.059 m and 0.088 m (the housing

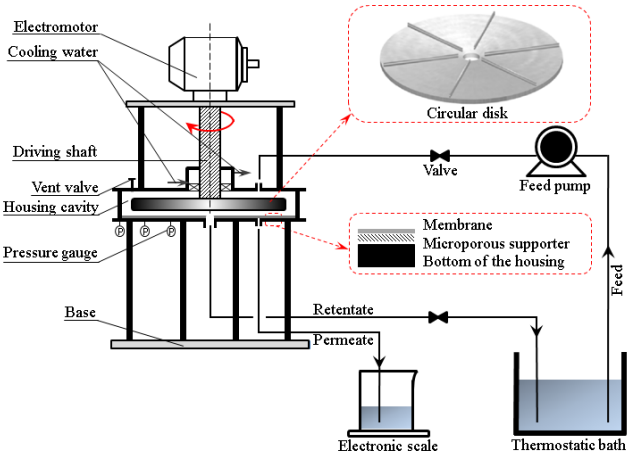

Figure 1. The diagram of the shear-induced PAUF experimental device.

periphery) from center, respectively. The permeate outlet is located at 0.059 m from the center opposite the pressure gauges and retentate flows from the center of the back plate.

Hydrodynamic model consideration

The shear rate on the local membrane, also called fluid velocity gradient (s^{-1}), has been analogized by previous study with Navier-Stokes equations (Bouzerar, et al., 2000) and can be converted as follows:

Turbulence:

$$\gamma = 0.029\upsilon^{-0.8}(k\omega)^{1.8}r^{1.6} \quad (1)$$

Laminar:

$$\gamma = 0.77\upsilon^{-0.5}(k\omega)^{1.5}r \quad (2)$$

were υ is the fluid kinematic viscosity (m^2/s). $k\omega$ is the angular velocity of the main region, where ω the disk angular velocity (rad/s) and k the velocity factor. r represents the distance from disk center (m). ω can be calculated by $\omega=30N/\pi$, in which N is the disk rotating speed (rpm, revolutions per minute). The dimensionless parameter k, always less than 1, illustrates the tracking ability of solution with rotating disk and only relates to the device geometry. Generally, a k value closer to 1 engenders stronger turbulent motion near the membrane surface. In addition, the flow transition of laminar-turbulence can be defined by the local Reynolds number Re ($=k\omega r^2/\upsilon$) attained to be about 2×10^5 (Bouzerar, et al., 2000). And the further investigation of shear stability as well as metal separation was carried out mainly in the turbulent state.

The formula of local pressure distribution on the membrane assuming that permeate is atmospheric has been derived below (Torras, et al., 2009):

$$P = 0.5\rho(k\omega r)^2 + P_o \quad (3)$$

where P_o is the initial pressure (kPa) measured at the membrane rim when the disk is not rotating. ρ is the fluid density (kg/m^3). And k value can be obtained by putting peripheral pressure P_p (monitored by the pressure gauge in the membrane rim; $r=r_m$, r_m is the membrane external radius, also equal to 1/2 of the housing inner diameter, 0.088 m) at different disk angular velocity ω into above equation. According to our previous study, k value of a circular disk with six radial vanes was calculated to be 0.79.

The permeation coefficient F ($L\cdot m^{-2}\cdot s^{-1}\cdot Pa^{-1}$), which reflects the membrane permeability and can indirectly reveal the membrane fouling degree, denotes the permeate flux per unit pressure and can be obtained by Darcy's law:

$$F = \frac{J}{P} = \frac{1}{\mu R_t} = \frac{1}{\mu\left(R_f + R_p + R_m\right)} \quad (4)$$

where J is the permeate flux ($L\cdot m^{-2}\cdot s^{-1}$), μ is the dynamic viscosity (Pa·s), and P is the pressure of the membrane surface (gage pressure). R_t is the total process resistance (m^{-1}). The R_f and R_p represent the resistance of membrane fouling and concentration polarization, respectively, R_f and R_p can be neglected at high enough shear rate (Tang and Qiu, 2018). R_m is the membrane resistance.

In operation, the membrane surface will be divided into a complexation region ($r_o \le r < r_c$) and a dissociation region ($r_c \le r < r_m$) when the disk rotation speed is large enough. Here r_o is the inner radius of the membrane, 0.005 m. r_c is defined as the critical radius, at which the dissociation of the PMA-metal complex exactly occurs. In the complexation region, the complex is stable and the entire filtration process can be considered as a general PAUF process; in the dissociation region, the PMA-metal complexes are dissociated by high shear. r_c can be simplified as below (Gao, et al., 2017; Tang and Qiu, 2018):

$$r_c^4 + \frac{4P_o}{\rho k^2\omega^2}r_c^2 = \frac{c_{dis}-c_p}{c_{dis}-c_{com}}\left(r_m^4 + \frac{4P_o r_m^2}{\rho k^2\omega^2}\right) + \frac{c_p - c_{com}}{c_{dis}-c_{com}}\left(r_o^4 + \frac{4P_o r_o^2}{\rho k^2\omega^2}\right) \quad (5)$$

where c_p, c_{com} and c_{dis} represent the concentration of metal in the permeate, complexation region and dissociation region, respectively. c_{dis} can be considered equal to the feed concentration c_f because all the PMA-metal complexes in the dissociation region are decomplexed by high shear, releasing only free PMA anions and metal cations. When $r_c=r_m$ the decomplexation exactly starts, we can obtain the critical shear rate γ_c by inserting r_m and the ω_c under this condition into the former Eq. (1) and Eq. (2). Particularly, γ in practice should be as large as possible to restrain the polarized membrane fouling and enhance the permeate flux, but must not exceed γ_c since an exorbitant shear rate will enlarge the dissociation area and cause a remarkable decline of rejection of metal ions. γ_c can give a guidance for the election of a transportation pump and the process design of dynamic filtration system.

The selective separation coefficient of Mn(II) and Cd(II) is universally defined as follow:

$$\beta_{Mn/Cd} = \frac{1-R_{Mn}}{1-R_{Cd}} \quad (6)$$

where R is the rejection of metal components. The higher β value ensures the greater separation performance of different metals.

Materials and analytical methods

All chemicals are reagent grade products. PMA aqueous solution was prepared to 1 g/L with ultrapure water, purchased from Xinqi Chemical Industries, Ltd (China). The average molecular weight of PMA is 70 kDa, and the molecular structure of PMA is given in Fig. 2. Aqueous solution containing Mn(II) and Cd(II) was prepared with $MnSO_4$ and $CdSO_4$, purchased from Xilong Chemical Co., Ltd (China). The initial concentrations of Mn(II) and Cd(II) were both 10 mg/L.

Metal concentration in the feed and permeate was measured by an ICP-OES (Optima 8000, Perkin Elmer, USA) or an ICP-MS (series 2, Thermo Fisher, USA). The pH was gauged with a digital display pH meter (PHS-25, China). The viscosity of test fluid was measured with an ubbelohde viscometer (MC-77, China).

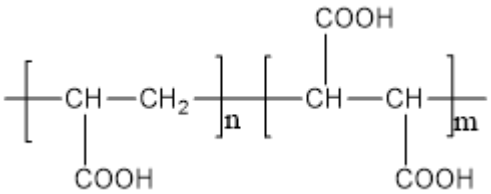

Figure 2. The structure of maleic acid-acrylic acid copolymer (PMA).

Procedure of complexation and ultrafiltration tests

In the complexation test, PMA solution and metal aqueous solution were successively poured into a 4 L bucket and the mixed solution was made up to 3 L with ultrapure water. After adjusting the solution pH to a desired value via 0.1 M hydrochloric acid or sodium hydroxide, the mixed solution was stirred for 2 h at 25 °C. In the ultrafiltration test, an original membrane was used for the entire test. The PMA-metal complex solution was put into a thermostatic bath. The Feed was delivered by a peristaltic pump running at constant flow rate to fill the housing cavity. It was supplied for the system after shutting the vent valve. Retentate was delivered to the feed tank and the permeate was collected in a beaker. The rotating disk was driven by an electromotor at a series of rotating speeds ranging from 0 to 3000 rpm. A series of P/Ms (1, 5, 9, 13), pHs (2, 3, 4, 5, 6, 7, 8) and disk rotating speeds (ranging from 0 to 3000 rpm) were independently increased to study the effects on metal rejection. Each sample was recorded when the permeate flux became stable after varying the operating conditions.

RESULTS AND DISCUSSIONS

The permeation coefficient and transmembrane pressure at various rotating speeds

The variation of the transmembrane pressure P and the permeation coefficient F calculated by Eq. (4) with various disk rotating speeds N using 150 mg/L PMA solution was plotted in Fig. 3. In order to obtain a stabilized flux, each sampling interval was selected as 5-10 min at a certain rotating speed. Based on the solution viscosity and sampling position, the characteristic rotating speed that defines the laminar-turbulence transition was obtained by $Re = k\omega r^2/\upsilon = 2\times10^5$ to be about 570 rpm.

Evidently, the P in Fig. 3 showed a parabolic uptrend with the increasing of rotating speed N. Across the whole test, almost no pressure drop was observed, suggesting that the dynamic PAUF with the RDM module could provide high enough driving force to improve the total process efficiency. Additionally, F showed a slow increase as N continued to rise and eventually maintained stable at a high level, though it was relatively low at 0 rpm owing to the accumulation of a polarization layer. Moreover, the total resistance R_t of PMA solution was calculated by inserting the F data into Eq. (4) and it was compared with that of ultrapure water in Fig. 4. Owing to no resistance of polarization R_p and fouling R_f, R_t, independent of disk rotation and maintained stable at R_m for ultrapure water, was 2.018×10^{12} m^{-1}. As shown in Fig. 4, when using PMA solution as test fluid, R_t decreased and gradually approached to R_m as N continued to increase, implying the final absence of any polarization layer or membrane fouling on the surface of the membrane. Compared with the laminar flow (N<570 rpm), the flow in turbulence (N>570 rpm) generated much less R_f and R_p, which indicated that the RDM module working at high enough disk rotation can practically depress or even eliminate the R_f and R_p to ensure a substantially stable permeation coefficient (Tu, et al., 2009).

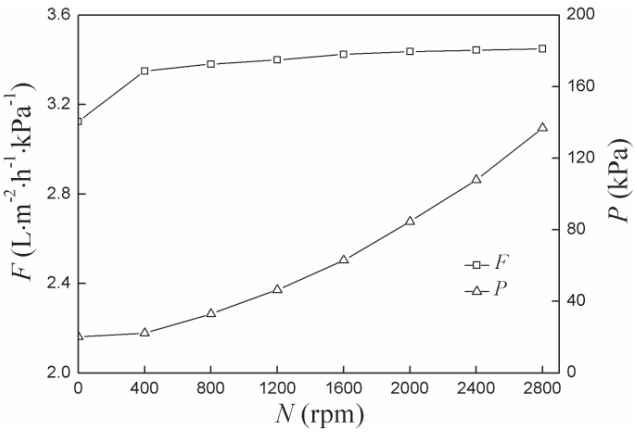

Figure 3. The variation of pressure P (gage pressure) and permeation coefficient F using PMA solution with disk rotary speed (initial PMA concentration, 150 mg/L; 25 °C; initial pressure, 20 kPa).

Distribution of shear rate on the membrane surface

In order to understand the shear effect of the RDM module on the flow in the housing cavity, the

distribution of shear rate along the membrane radius at different disk rotating speeds (1000~3000 rpm) when using 150 mg/L PMA solution was investigated by CFD calculation in the turbulent state. As shown in Fig. 5, higher rotating speed induced greater shear rate γ. As well, γ increased following along the radial direction from the membrane center to the membrane periphery. This implied that the position further from the center of the membrane generated a larger radial velocity gradient, which enhanced the turbulent motion and contributed to the axial filtration process. In addition, since the flow on the stationary wall of the housing cavity (r=0.088 m) was decelerated, which was less stable, the γ close to the membrane periphery (r=0.088 m) had a slight deviation from the original uptrend and decreased a little.

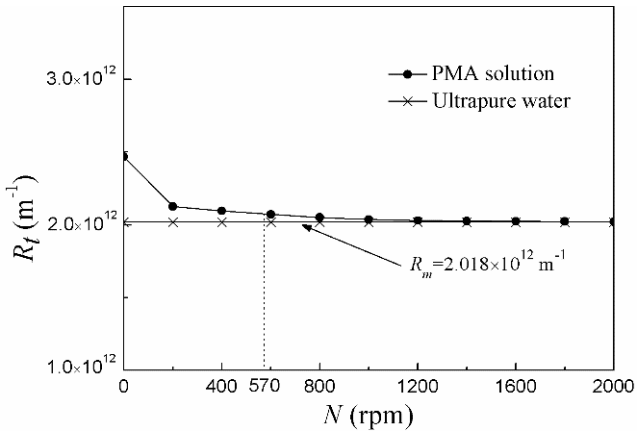

Figure 4. Comparison of the total resistance R_t of PMA solution and ultrapure water at various disk rotary speeds (initial PMA concentration, 150 mg/L; 25 °C; initial pressure, 20 kPa).

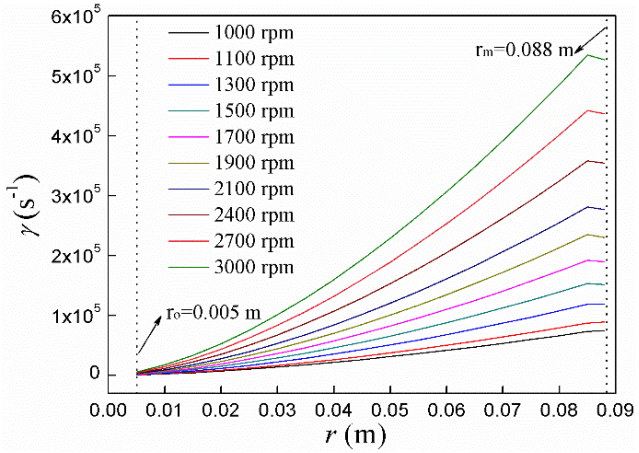

Figure 5. Radial distribution of shear rate on the membrane surface at various disk rotary speeds (initial PMA concentration, 150 mg/L; 25 °C; initial pressure, 20 kPa).

Variations of Mn(II) and Cd(II) rejection with pH and P/M

It is believed that the solution pH has a great effect on the size and shape of polymer chains, as well as the formation of polymer-metal complexes (Juang and Chen, 1996). Moreover, P/M also affects the rejection of metal ions. Low P/M lets certain free uncomplexed metal ions exist in solution, whereas high P/M leads to the increase of solution viscosity and may attenuate the membrane flux. Fig. 6 displayed the variation of single Mn(II) and Cd(II) rejection with pH and P/M at 300 rpm. In the figure, the rejection had a sharp increase at fixed P/M when pH varied from 2 to 6 and was almost stable at pH>6, which agreed well with a previous study (Cañizares, et al., 2008). This can be explained by a greater amount of deprotonated carboxylic groups on PMA chains at higher pH, causing a higher bonding capacity between PMA and metals. The basically unchanged rejection when pH exceeded 6 might be due to complete complexation, leaving less free Mn(II) or Cd(II) in solution, which would be mostly precipitated as retentate. In addition, the Cd(II) rejection was higher than for Mn(II) at the same pH and P/M, intimating the greater relative affinity of carboxyl for Cd(II) than for Mn(II). To take the main factors of complexing formation and solution viscosity into consideration, the optimal complexation condition was set at pH 6 and P/M 9, under which the Mn(II) and Cd(II) rejections were up to 99.1% and 99.7%, respectively.

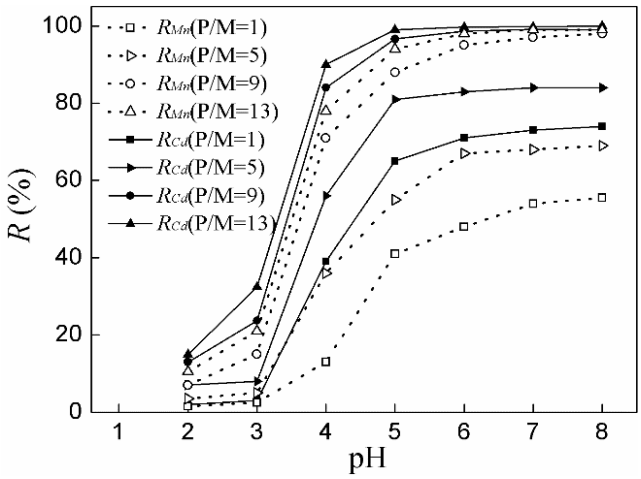

Figure 6. Variation of Mn(II) and Cd(II) rejection with pH at different P/Ms (initial metal concentration, 10 mg/L; constant disk rotary speed, 300 rpm; 25 °C; initial pressure, 20 kPa).

The shear stability of PMA-Mn and PMA-Cd complexes

For exploring the shear stability of PMA-metal complexes, the effect of disk rotating speed N on single Mn(II) and Cd(II) rejection at pH 4, 5, 6 and the same P/M 9 was investigated. As shown in Fig. 7, the

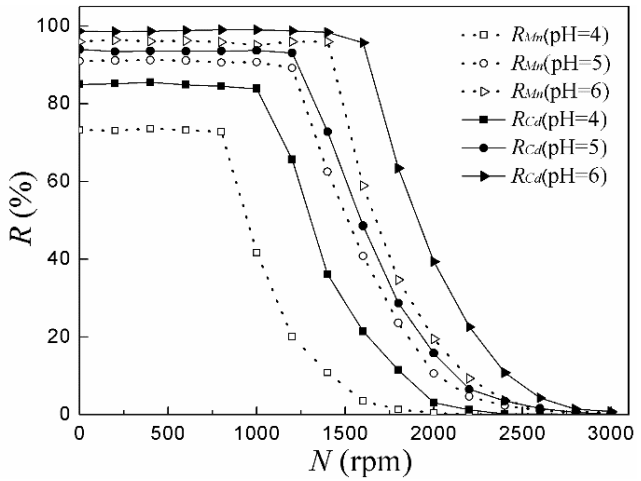

Figure 7. Effect of rotary speed on Mn(II) and Cd(II) rejection at pH 4, 5, 6 (P/M, 9; initial metal concentration, 10 mg/L; 25 °C; initial pressure, 20 kPa).

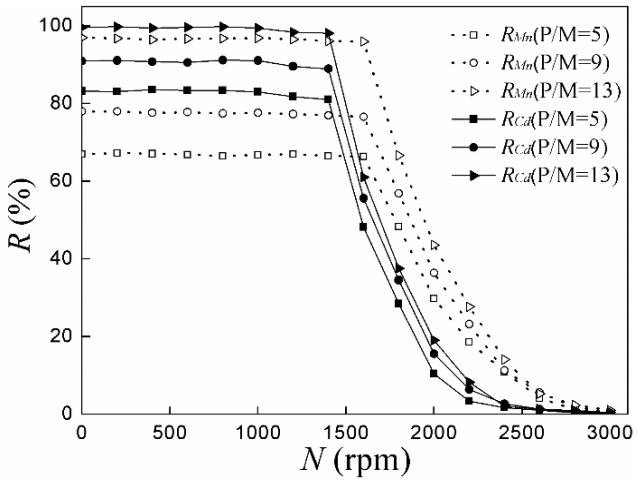

Figure 8. Effect of rotary speed on Mn(II) and Cd(II) rejection at P/M 5, 9, 13 (pH value, 6; initial metal concentration, 10 mg/L; 25 °C; initial pressure=20 kPa).

rejection was stable on a high level at the beginning, then it reached a critical value and sharply decreased, indicating that the PMA-Mn or PMA-Cd complex started to dissociate and the dissociation region got larger from the membrane periphery to membrane center with the sustained increase of N beyond the critical rotating speed N_c. From Fig. 7, the N_c of Mn(II) were attained at 800, 1200 and 1400 rpm at pH 4, 5, 6, respectively; while those of Cd(II) at the same pHs were attained at 1000, 1250 and 1500 rpm, respectively. The higher N_c at higher pH indicated that higher pH can ensure greater shear stabilities of PMA-metal complexes, and this fact could be explained as follows: A higher pH induces more deprotonated carboxylic groups of PMA, providing sufficient ligands to drive the complexation reaction of PMA with free metal cations (Tang and Qiu, 2018). This augments the complexity of the coordination mode between polymer and metals (Bazzicalupi, et al., 2010), which can make the formed PMA-metal complexes more stable. Furthermore, Fig. 8 demonstrated the variation of single Mn(II) and Cd(II) rejection at P/M 5, 9, 13 and at various rotating speeds under pH 6. As expected, the N_c of Mn(II) or Cd(II) at three P/Ms were almost the same, and the decreasing trends of N_c were very close to each other. It could be inferred that the shear stability of PMA-metal complex was essentially affected by pH rather than P/M.

Fig. 9 illustrated the fitting curve of the associated critical radius r_c calculated by Eq. (5) to reveal the expansion mechanism of the dissociation region. As shown in the figure, r_c at the corresponding N_c dropped from r_m and gradually decreased with N increasing. The fact is that r_c of PMA-Mn at the same pH was always lower than PMA-Cd qualified the better stability of PMA-Cd compared with PMA-Mn. What is more, the related critical shear rates γ_c of two PMA-metal

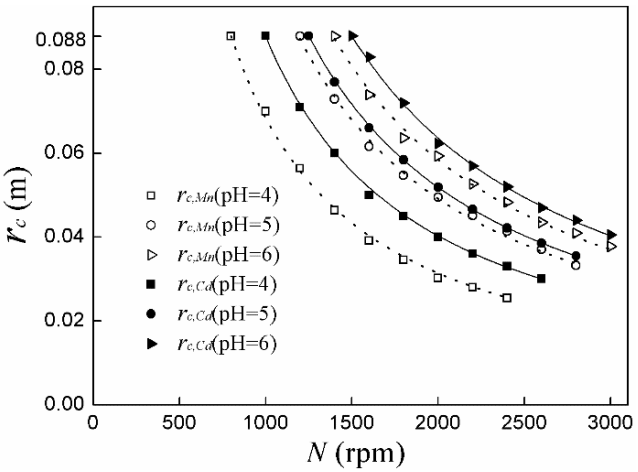

Figure 9. Variation of critical radius r_c (Mn) and r_c (Cd) with disk rotary speed (P/M, 9; initial metal concentration, 10 mg/L; 25 °C; initial pressure, 20 kPa).

complexes at pH 4, 5, 6 were calculated according to Eq. (1) in the turbulent state, and the relationship between r_c and N was obtained to understand the shear instability mechanism, which was displayed in Table 1. It can be concluded from Table 1 that a fixed pH assures a constant γ_c, a shear rate beyond γ_c decreases r_c and enlarges the zone of dissociation region. Moreover, Mn(II) and Cd(II) may be selectively separated via the difference of shear stability between PMA-Mn and PMA-Cd complexes. To sum up, this section could provide a certain theoretical guidance for the choice of a delivery pump in the industrial operation of dynamic PAUF.

Determination of the selective separation coefficient of Mn(II) and Cd(II)

For determining the optimal separation condition, the variation of the selective separation coefficients of

Table 1. γ_c of PMA-Mn and PMA-Cd as well as the correlations of r_c and N at different pHs.

Complexes	pH	N_c (rpm)	γ_c (s^{-1})	Fitting equation	Regression coefficient (R^2)
PMA-Mn	4	800	5.32×10^4	$r_c=162.27N^{-1.125}$	0.9975
	5	1200	1.10×10^5	$r_c=254.28N^{-1.125}$	0.9891
	6	1400	1.47×10^5	$r_c=302.21N^{-1.125}$	0.9959
PMA-Cd	4	1000	7.95×10^4	$r_c=208.40N^{-1.125}$	0.9961
	5	1250	1.19×10^5	$r_c=268.21N^{-1.125}$	0.9982
	6	1500	1.65×10^5	$r_c=329.14N^{-1.125}$	0.9997

Mn(II) and Cd(II) $\beta_{Mn/Cd}$ under different disk rotating speeds N at pH 4, 5, 6 and P/M 9 was shown in Fig. 10. At a given pH, the $\beta_{Mn/Cd}$ stayed at a low level close to 0 at the beginning, and then it sharply increased to a peak value. This could be ascribed to PMA-Mn begining to dissociate when N reached the critical state and Mn(II) concentration in the permeate increasing, resulting in the great disparity between Mn(II) and Cd(II) rejection. As N continued to rise, the dissociation of PMA-Cd started, and the Mn(II) rejection was basically low at this time, causing the sharp drop of $\beta_{Mn/Cd}$ from its peak value to nearly 0. As well, the peak value at pH 6 was relatively larger, which revealed that higher pH was more suitable for the selective separation of Mn(II) and Cd(II). From Fig. 10, the peak values of $\beta_{Mn/Cd}$ at pH 4, 5, 6 were obtained at 950, 1300 and 1450 rpm, respectively. And the corresponding shear rates at three pHs were calculated to be 7.25×10^4, 1.28×10^5 and 1.55×10^5 s^{-1}, which could be helpful for the synthetic parameter selection of a centrifugal pump in the practical separation of Mn(II) and Cd(II) during a shear enhanced PAUF process. Accordingly, P/M 9, pH 6 and 1450 rpm were selected to be the optimal condition for further tests of shear induced dissociation coupled with ultrafiltration.

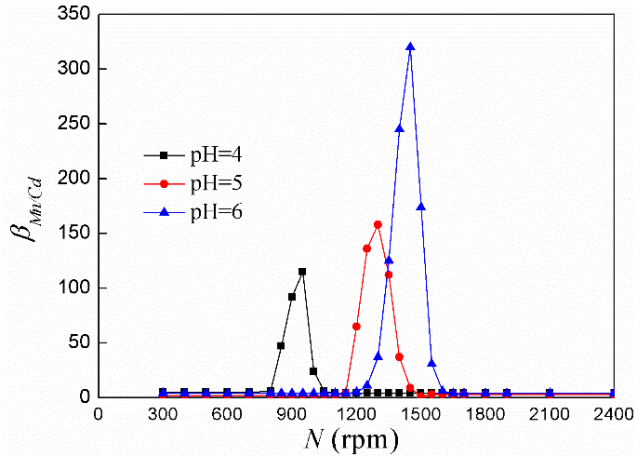

Figure 10. Effect of disk rotary speed on the selective separation coefficient of Mn/Cd at different pHs (P/M, 9; initial metal concentration, 10 mg/L; 25 °C; initial pressure, 20 kPa).

Shear induced dissociation coupled with ultrafiltration

The contents of Mn(II) and Cd(II) as well as pH value in simulated wastewater, which was prepared according to real water around the manganese mining area, has been characterized in Table 2. Since P/M affected little the stability of PMA-metal complexes, enough PMA was added to fix the $P/M_{Mn(II)+Cd(II)}$ at 9. At the beginning, the ultrafiltration test of simulated wastewater was conducted at 1450 rpm to dissociate PMA-Mn and release Mn(II). Later, the disk rotating speed N was risen up to 1600 rpm to dissociate PMA-Cd and displace the remaining Cd(II). During the consecutive process, permeate was continuously discharged and retentate flowed back to the feed bath to concentrate the dissociated PMA. Feed fluid in the bath was made up by putting in moderate ultrapure water to maintain the constant volume. All the results were displayed in Fig. 11. Herein, c_i/c_o represented the ratio of timely concentration to initial concentration, and V_R denoted the volume ratio of make-up water to the initial feed. Obviously when V_R varied from 0 to 21, the c_i/c_o of Mn(II) and Cd(II) at two shear fields were separately diminished from 1 to practically 0, suggesting the excellent removal rate of two metals and exceptional separation effect. Furthermore, the c_i/c_o of PMA produced from the decomplextion of PMA-Mn and PMA-Cd complexes were constant at 1 throughout whole test, which signified the great stability of PMA structure regardless of high shear. For responding the goal of organic reutilization in cyclic economy, the PMA was finally regenerated by concentration.

The comparison of Mn(II) rejection using regenerated PMA and original PMA at the same experimental conditions was shown in Fig. 12. It was observed from Fig. 12 that the Mn(II) rejection of regenerated PMA diminished very little and was even up to 98.4% compared to 99.1% of original PMA at pH 6 and P/M 9. The rather low Mn(II) rejection of regenerated PMA compared with that of original PMA was explained as follows: Though the shear induced separation test gave a good effect, there remained a few free Cd(II) and undissociated PMA-Cd in the

Table 2. The heavy metal concentration of real wastewater after pre-treatment.

Water streams	Mn(II) (mg/L)	Cd(II) (mg/L)	pH value
Real wastewater	451.5	104.8	3
After chemically precipitating methods	14.9	9.2	6

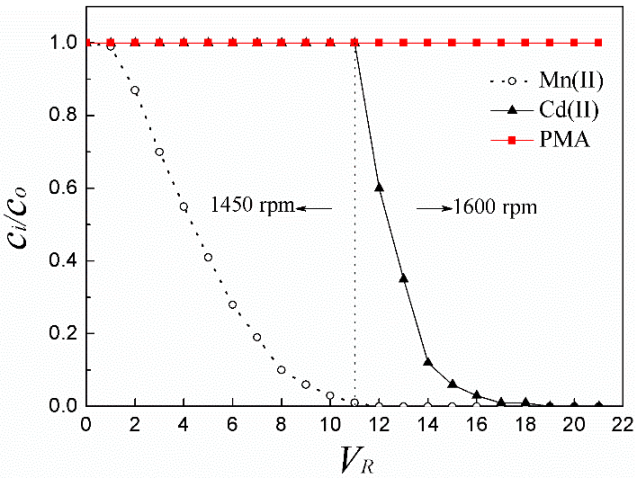

Figure 11. The variation curve of Mn(II), Cd(II) and PMA concentration at two shear fields (pH 6; P/M, 9; initial Mn(II) concentration, 14.9 mg/L; initial Cd(II) concentration, 9.2 mg/L; 25 °C; initial pressure, 20 kPa).

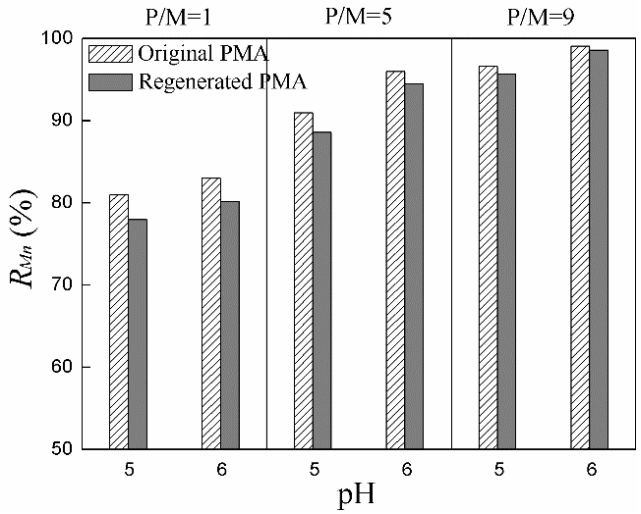

Figure 12. The comparison of Mn(II) rejection using regenerated PMA and original PMA at pH 5, 6 and P/M 1, 5, 9 (initial metal concentration, 10 mg/L; 25 °C; initial pressure, 20 kPa).

concentrate. The former could compete with Mn(II) to bond with the carboxyl, and the latter made the real content of functional PMA in the regenerated solution slightly lower than that of the original PMA under same P/M. From this section, the method of shear induced dissociation coupled with ultrafiltration could efficiently separate Mn(II) and Cd(II), as well as enable the complexing agent to be recycled.

CONCLUSIONS

The present study mainly investigated the shear stability of PMA-Mn and PMA-Cd complex as well as selective separation of Mn(II) and Cd(II) in a shear enhanced PAUF system equipped with a RDM module. In this system, the high shear rate indeed lessened or even eliminated the concentration polarization and membrane fouling to ensure a substantially constant and high permeation coefficient. The distribution of shear rate on the membrane surface was explored, demonstrating that the shear rate increased along the radial direction. Additionally, the optimal complexation condition was found to be solution pH 6 and P/M 9, at which both the rejection of Mn(II) and Cd(II) reached more than 99%. The shear stability of PMA-Mn and PMA-Cd complexes as a function of solution pH was mainly studied, indicating that the related critical rotating speeds were larger at higher pHs. The corresponding critical shear rates γ_c of PMA-Mn and PMA-Cd complexes at three pHs were obtained and results revealed that the structure of PMA-Cd complex was relatively more stable than PMA-Mn complex. In order to stabilize the permeation coefficient to improve process efficiency but not break the stability of the polymer-metal complex in the shear field, the shear rate should be high enough but not exceed γ_c, which confirms the feasibility of dynamic filtration with a RDM module and can be theoretically helpful for the selection of a feed pump as well as control of rotating speed in practical operation of PAUF. Moreover, based on the difference of shear stability between PMA-Mn and PMA-Cd complexes, the selective separation of Mn(II) and Cd(II) was finally conducted by shear induced dissociation coupled with ultrafiltration. The results indicated that SID-UF achieved a good separation effect, and the PMA was regenerated. Overall, this study provided a green and efficient treatment for the removal of Mn(II) and Cd(II), as well as confirming the novel idea to separate or concentrate the materials from wastewater based on the difference of shear stability between various polymer-material complexes.

NOMENCLATURE

Roman letters

c_o	Initial concentration of component (mg/L)
c_f	Metal concentration in the feed (mg/L)
c_p	Metal concentration in permeate (mg/L)
k	Velocity factor
r	Distance from membrane center (m)
r_m	Membrane external radius (m)
r_o	Membrane inner radius (m)
r_c	Critical radius (m)
P	Pressure on membrane (kPa)
P_o	Initial pressure (kPa)
P_o^p	Peripheral pressure (kPa)
J^p	Permeate flux ($L \cdot m^{-2} \cdot h^{-1}$, $L \cdot m^{-2} \cdot s^{-1}$)
F	Permeation coefficient ($L \cdot m^{-2} \cdot h^{-1} \cdot kPa^{-1}$, $L \cdot m^{-2} \cdot s^{-1} \cdot Pa^{-1}$)
N	Disk rotating speed (rpm)

N_c Critical disk rotating speed (rpm)
R_t Total resistance (m^{-1})
R_p Resistance of concentration polarization (m^{-1})
R_f Resistance of membrane fouling (m^{-1})
R_m Membrane intrinsic resistance (m^{-1})
R Rejection of component (%)
V_R Volume ratio of make-up water to the initial feed

Greek letters

υ Kinematic viscosity (m^2/s)
μ Dynamic viscosity (Pa·s)
ω Disk angular velocity (rad/s)
ρ Fluid density (kg/m^3)
γ Shear rate on the membrane surface (s^{-1})
γ_c Critical shear rate (s^{-1})
$\beta_{Mn/Cd}$ Selective separation coefficient of Mn (II) and Cd (II)

ACKNOWLEDGMENT

This work was supported by the National Science Foundation of China (Project 21476265).

REFERENCES

Bazzicalupi, C., Biagini, S., Bianchi, A., Faggi, E., Gratteri, P., Mariani, P., Pina, F., Valtancoli, B. Binding of H^+ and Zn(II) ions with a new fluorescent macrocyclic phenanthrolinophane. Dalton Transactions, 39, 10128-10136 (2010). https://doi.org/10.1039/c0dt00534g

Bouzerar, R., Ding, L. H., Jaffrin, M. Y. Local permeate flux-shear-pressure relationships in a rotating disk microfiltration module: implications for global performance. Journal of Membrane Science, 170, 127-141 (2000). https://doi.org/10.1016/S0376-7388(99)00348-8

Cañizares, P., Pérez, A., Camarillo, R., Mazarro, R. Simultaneous recovery of cadmium and lead from aqueous effluents by a semi-continuous laboratory-scale polymer enhanced ultrafiltration process. Journal of Membrane Science, 320, 520-527 (2008). https://doi.org/10.1016/j.memsci.2008.04.043

Demey, H., Vincent, T., Guibal, E. A novel algal-based sorbent for heavy metal removal. Chemical Engineering Journal, 332, 582-595 (2018). https://doi.org/10.1016/j.cej.2017.09.083

Frappart, M., Akoum, O., Ding, L. H., Jaffrin, M. Y. Treatment of dairy process waters modelled by diluted milk using dynamic nanofiltration with a rotating disk module. Journal of Membrane Science, 282, 465-472 (2006). https://doi.org/10.1016/j.memsci.2006.06.005

Gao, J., Qiu, Y. R., Hou, B., Zhang, Q., Zhang, X. D. Treatment of wastewater containing nickel by complexation- ultrafiltration using sodium polyacrylate and the stability of PAA-Ni complex in the shear field. Chemical Engineering Journal, 334, 1878-1885 (2018). https://doi.org/10.1016/j.cej.2017.11.087

Geckeler, K. E., Volchek, K. Removal of hazardous substances from water using ultrafiltration in conjunction with soluble polymers. Environmental Science & Technology, 30, 725-734 (1996). https://doi.org/10.1021/es950326l

Jaffrin, M. Y. Dynamic shear-enhanced membrane filtration: A review of rotating disks, rotating membranes and vibrating systems. Journal of Membrane Science, 324, 7-25 (2008). https://doi.org/10.1016/j.memsci.2008.06.050

Jarvinen, G. D., Smith, B. F., Robison, T. W., Kraus, K. M., Thompson, J. A. Removal and recovery of metal ions from process and waste streams using polymer filtration, United Engineering Foundation Conference on Metal Separation Technologies beyond 2000: Integrating Novel Chemistry and Processing, Hawaii (1999).

Juang, R. S., Chen, M. N. Retention of copper(II)-EDTA chelates from dilute aqueous solutions by a polyelectrolyte-enhanced ultrafiltration process. Journal of Membrane Science, 119, 25-37 (1996). https://doi.org/10.1016/0376-7388(96)00101-9

Juang, R. S., Chiou, C. H. Ultrafiltration rejection of dissolved ions using various weakly basic water-soluble polymers. Journal of Membrane Science, 177, 207-214 (2000). https://doi.org/10.1016/S0376-7388(00)00464-6

Juang, R. S., Shiau, R. C. Metal removal from aqueous solutions using chitosan-enhanced membrane filtration. Journal of Membrane Science, 165, 159-167 (2000). https://doi.org/10.1016/S0376-7388(99)00235-5

Luo, J. Q., Ding, L. H., Wan, Y. H., Paullier, P., Jaffrin, M. Y. Application of NF-RDM (nanofiltration rotating disk membrane) module under extreme hydraulic conditions for the treatment of dairy wastewater. Chemical Engineering Journal, 163, 307-316 (2010). https://doi.org/10.1016/j.cej.2010.08.007

Molinari, R., Argurio, P., Poerio, T. Comparison of polyethylenimine, polyacrylic acid and poly(dimethylamine-co-epichlorohydrin-co-ethylenediamme) in Cu^{2+} removal from wastewaters by polymer-assisted ultrafiltration. Desalination, 162, 217-228 (2004). https://doi.org/10.1016/S0011-9164(04)00045-1

Molinari, R., Argurio, P., Poerio, T. Ultrafiltration of polymer-metal complexes for metal ion removal from wastewaters. Macromolecular Symposia, 235, 206-214 (2006). https://doi.org/10.1002/masy.200650325

Pacini, V. A., Ingallinella, A. M., Sanguinetti, G. Removal of iron and manganese using biological roughing up flow filtration technology. Water Research, 39, 4463-4475 (2005). https://doi.org/10.1016/j.watres.2005.08.027

Qiu, Y. R., Mao, L. J. Removal of heavy metal ions from aqueous solution by ultrafiltration assisted with copolymer of maleic acid and acrylic acid. Desalination, 329, 78-85 (2013). https://doi.org/10.1016/j.desal.2013.09.012

Sahabi, D. M., Takeda, M., Suzuki, I., Koizumi, J. Removal of Mn^{2+} from water by "aged" biofilter media: the role of catalytic oxides layers. Journal of Bioscience & Bioengineering, 107, 151-157 (2009). https://doi.org/10.1016/j.jbiosc.2008.10.013

Shafaei, A., Rezayee, M., Arami, M., Nikazar, M. Removal of Mn^{2+} ions from synthetic wastewater by electrocoagulation process. Desalination, 260, 23-28 (2010). https://doi.org/10.1016/j.desal.2010.05.006

Sharma, Y. C., Sharma, U., Singh, S. N., Paras, Gode, F. Fly ash for the removal of Mn(II) from aqueous solutions and wastewaters. Chemical Engineering Journal, 132, 319-323 (2007). https://doi.org/10.1016/j.cej.2007.01.018

Taffarel, S. R., Rubio, J. On the removal of Mn^{2+} ions by adsorption onto natural and activated Chilean zeolites. Minerals Engineering, 22, 336-343 (2009). https://doi.org/10.1016/j.mineng.2008.09.007

Tang, S. Y., Qiu, Y. R. Removal of copper(II) ions from aqueous solutions by complexation-ultrafiltration using rotating disk membrane and the shear stability of PAA-Cu complex. Chemical Engineering Research & Design, 136, 712-720 (2018). https://doi.org/10.1016/j.cherd.2018.06.030

Torras, C., Pallares, J., Rigard, G. V., Jaffrin, M. Y. Numerical simulation of the flow in a rotating disk filtration module. Desalination, 235, 122-138 (2009). https://doi.org/10.1016/j.desal.2008.02.006

Tu, Z. H., Ding, L. H., Frappart, M., Jaffrin, M. Y. Studies on treatment of sodium dodecyl benzene sulfonate solution by high shear ultrafiltration system. Desalination, 240, 251-256 (2009). https://doi.org/10.1016/j.desal.2008.01.051

Viadero, R. C., Masciola, D. A., Reed, B. E., Vaughan, R. L. Two-phase limiting flux in high-shear rotating ultrafiltration of oil-in-water emulsions. Journal of Membrane Science, 175, 85-96 (2000). https://doi.org/10.1016/S0376-7388(00)00408-7

Ye, C. S., Yang, H., Lin, J. Y., Zeng, H. M., Yu, F. Study on ion exchange property of removing Mn^{2+} and Fe^{2+} in groundwater by modified zeolite. Desalination & Water Treatment, 30, 114-121 (2011). https://doi.org/10.5004/dwt.2011.1927

Zeng, J. X., Sun, X. H., Zheng, L. F., He, Q. C., Li, S. Recovery of tungsten(VI) from aqueous solutions by complexation-ultrafiltration process with the help of polyquaternium. Chinese Journal of Chemical Engineering, 20, 831-836 (2012). https://doi.org/10.1016/S1004-9541(12)60406-6